Slippage dynamics of confined water in graphene oxide capillaries

H. G. Kalashami,[1] M. Neek-Amal,[2] and F. M. Peeters[1]
[1]*Departement Fysica, Universiteit Antwerpen, Groenenborgerlaan 171, Antwerpen B-2020, Belgium*
[2]*Department of Physics, Shahid Rajaee Teacher Training University, 16875-163 Lavizan, Tehran, Iran*

(Received 27 March 2018; published 23 July 2018)

The permeation of water between neighboring graphene oxide (GO) flakes, i.e., 2D nanochannels, are investigated using a simple model for the GO membrane. We simulate the hydrophilic behavior of nanocapillaries and study the effect of surface charge on the dynamical properties of water flow and the influence of Na^+ and Cl^- ions on water permeation. Our approach is based on extensive equilibrium molecular dynamics simulations to obtain a better understanding of water permeation through charged nanochannels in the presence of ions. We found significant change in the slippage dynamics of confined water such as a profound increase in viscosity/slip length with increasing charges over the surface. The slip length decreases one order of magnitude (i.e., 1/30) with increasing density of surface charge, while it increases by a factor of 2 with ion concentration. We found that commensurability induced by nanoconfinement plays an important role on the intrinsic dynamical properties of water.

DOI: 10.1103/PhysRevMaterials.2.074004

I. INTRODUCTION

Nanocapillaries play an important role in the design of materials for filtration and separation because of their unusual fundamental behavior arising at the molecular scale [1,2]. Stacked graphene oxide (GO) sheets are the oxidized form of hydrophilic graphene nanosheets with a high density of oxygen containing functional groups (e.g., hydroxyl, carboxyl, carbonyl, and epoxy groups). Individual GO flakes are exfoliated by dissolving GO in water with the help of ultrasonication and bulk residues. The space between the neighboring GO flakes creates 2D nanochannels that may allow water to pass through while rejecting the flow of contaminants. The ultrafast permeation of water through GO membranes has led to a large interest in the development of nanofiltration membranes. Nair *et al.* observed that a sub-micrometer-thick GO membrane can be completely impermeable to liquids, vapors, and gases, including helium, whereas it allows unimpeded permeation of water [3]. This is very promising for water desalination and gas selection applications, and for experimental and theoretical studies of nanofluidics [4]. The nanoscale GO membranes can be used to achieve accurate and tunable ion sieving [5].

Numerous studies based on molecular dynamics (MD) simulations identified key factors that affect transport through nanocapillaries [1,2,6]: the breakdown of uniform water density; the water-solid wall slip length which is found to be much larger than capillary sizes; dynamical properties different from bulk, etc. Despite recent progress, the molecular mechanisms underlying the diffusion of water in charged porous media (hydrophilic materials) and the interplay between the effects of a charged surface and ions are not understood so far.

The behavior of Na^+ and Cl^- ions in bulk water or at the interface of hydrophobic/hydrophilic media was widely investigated in recent works [7]. However, a few studies have addressed the effect of the concentration of ions on the dynamical properties of water in charged nanocapillaries [8]. Determining the slip length of water permeating through GO membranes is urgently needed because it will be helpful to understand the flow through nanocapillaries as mentioned in recent experimental studies [3,4,9–12]. In fact, the slip length ($L = \eta/\xi$) is a crucial parameter that determines water flow within nanochannels. Despite many reports on the slip length for hydrophobic surfaces [13], there are very few reports on the slip length over hydrophilic surfaces or charged surfaces. For instance Wei *et al.* reported two orders of magnitude reduction of the slip length of water in the presence of chemical functionalization and nanoconfinement in graphene oxides [14].

Here, we study systemically the influence of ion concentration and surface charge on the dynamical properties of confined water and elucidate the influence of capillary size. In particular, a mixture of H_2O, Na^+, and Cl^- inside a nanocapillary made of graphene layers will be investigated. We found a significant change in the water slip length versus surface charge while the ion concentration has much less influence on it. The charge distribution over graphene sheets mimics the microscopic nature of a GO membrane (see Appendix). The distributed charge plays the role of functional groups in graphene oxide. In the Appendix, we showed the consistency of this simple model. In fact, such a model can be promising because it ignores unnecessary details and reduces the complexity while allowing us to reproduce the essential physical features. In particular, commensurability effects result in clear oscillations in the dynamical properties of confined water which highlight the importance of accurate size control of the nanocapillaries.

II. MODEL AND METHODS

At the nanoscale a continuum-slip approach (based on solving the Navier-Stokes equation) is insufficient. The continuum hypothesis breaks down when the length scale of the nanofluidic system approaches the molecular scale. Since fluids are composed of molecules, one option is to calculate dynamical properties by computing the motion of the molecules.

Molecular dynamics (MD) simulations is a standard tool to investigate nanofluidics at molecular scales because it enables us to study molecular details of fluid flow (e.g., nanofluidics). Our methodology and models are suitable to allow MD simulations of nanoconfined water in the range of nanoseconds and are reliable enough to reproduce the relevant effects related to water permeation through nanocapillaries.

A. MD simulations

Using the large scale atomic/molecular massively parallel simulator LAMMPS [15], we investigated the impact of surface charges in the confining walls and ion hydration on the dynamical properties (i.e., diffusion, viscosity, and friction coefficient) of water confined inside graphene capillaries. Our simulated system contains two layers of graphene each with 680 carbons, i.e., our configuration unit cell has dimensions 42 Å(l_x) × 43 Å(l_y). The number of water molecules varies between 180 to 4640 depending on the interlayer separation h, i.e., capillary size. In order to add ions to the system, every two randomly selected H_2O molecules are replaced by an Na^+ and Cl^- ion, keeping the total net charge of the system zero. The graphene layers were fixed at their positions. The SPC/E model was employed to describe the water molecules [16].

The particles interact via Lennard-Jones (LJ) pair potentials using $\epsilon_C = 0.071224$ kcal mol^{-1}, $\sigma_C = 3.41$ Å, $\epsilon_{Na^+} = 0.130019$ kcal mol^{-1}, $\sigma_{Na^+} = 2.35$ Å, $\epsilon_{Cl^-} = 0.100143$ kcal mol^{-1}, and $\sigma_{Cl^-} = 4.40$ Å, and cross LJ potential parameters were obtained by the Lorentz-Berthelot combining rules [17,18].

The cutoff radius for the LJ potential was chosen at 10 Å. The NVT ensemble (Nose-Hoover thermostat) is used to keep the temperature at 300 K. Periodic boundary conditions are employed along x, y directions and the confinement was along the z direction. The particle-particle particle-mesh method was used to compute the long-range Coulomb interaction with a relative accuracy of 10^{-4}. Water bonds and angle was fixed by the SHAKE algorithm [19]. In all cases, the total density of water and ions was kept fixed at 1 g cm^{-3} and a timestep of 1 fs was chosen. After relaxing the system for 1 ns, the thermodynamical sampling was done for 5 ns to ensure the smoothness of the correlation function and to realize convergence to zero for large t. The volume of the capillary is defined by $l_x l_y \times (h - \sigma_{C-O})$. Here σ_{C-O} is subtracted to exclude the effective graphene interlayer distance of carbon-oxygen, i.e., the excluded volume effect.

In order to explore the impact of surface charges, we modeled the graphene oxide membrane by introducing excessive charge on some carbon atoms. Accordingly, we randomly assigned positive and negative charges (±e) to the atoms with an average surface charge density of σ; the total net charge on each graphene layer was set to zero. We ensured that the minimum distance between charges is 3 Å. Figure 1(a) gives a schematic view of the surface charge distribution over a graphene sheet, and Figs. 1(b) and 1(c) show corresponding top and side views where red and white colors refer to the water molecules, and Na^+ and Cl^- are shown by blue and cyan balls which are trapped between the two graphene layers (gray lines). The concentration of ions is given by $n_i/(n_i + n_w)$,

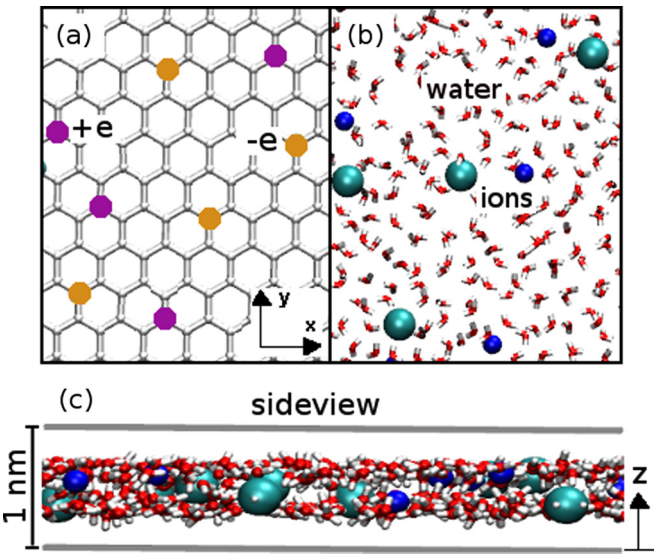

FIG. 1. The surface charge distribution over a graphene layer (a). Top (b) and side (c) view snapshots of ions (cyan and blue balls) mixture in water (red and white molecules) confined between a graphene capillary (gray lines). Periodic boundary conditions are employed in x and y directions and confinement was along the z axis.

where n_i and n_w refer to the number of ions and water molecules, respectively.

The average number of neighboring water molecules at radial distance r of an individual ion is evaluated by

$$n(r) = \frac{N}{V}\int_0^r g(r)\,4\pi r^2 dr\,, \tag{1}$$

where N/V is the total water density and $g(r)$ is the appropriate radial distribution function (RDF) between the ion and oxygen atoms. We used n_1 and n_2 as the number of water molecules within the first and second hydration shells, respectively.

B. Dynamical coefficients

Here we highlight the important details in the calculation of dynamical properties in the presence of confinement. There are two principal methods to explore the dynamical properties using equilibrium molecular dynamics simulations: direct method based on the Einstein relation—mean square approaches—and integrating the auto-correlation function (ACF) over time [20]. In the long time limit, these two methods are equivalent

$$\lim_{t\to\infty}\frac{1}{2t}[G(t) - G(0)]^2 = \int_0^\infty \langle \dot{G}(t_0)\dot{G}(t_0 + t)\rangle_{t_0} dt\,, \tag{2}$$

where $G(t)$ is any dynamical variable related to some particular transport coefficient, $\dot{G}(t)$ is the corresponding time derivative, and $\langle\,\rangle_{t_0}$ represents a canonical averaging. In fact, different transport properties can be evaluated using one of these two equivalent expressions.

Components of the diffusion coefficient D_α, where $\alpha = x, y, z$, can be determined by inserting the position $G(t) = r^\alpha(t)$ and velocity $\dot{G}(t) = v^\alpha(t)$ into Eq. (2). As a result, D_α

can be calculated using

$$D_\alpha = \lim_{t\to\infty} \frac{1}{2t}\langle [r^\alpha(t) - r^\alpha(0)]^2\rangle_i = \int_0^\infty \langle\langle v^\alpha(t_0)v^\alpha(t_0+t)\rangle_{t_0}\rangle_i dt\,, \quad (3)$$

where $\langle\,\rangle_i$ denotes averaging over all atoms [8,21]. Bulk diffusion coefficient (D) is computed as the average over all the components of D_α in Eq. (3). In the present study, we calculated the diffusion constants using the mean square displacement method taking one sample per 10 fs for the linear regression.

Similarly, the (shear) viscosity η can be determined from the Green-Kubo (GK) formula [22–24] that is based on the stress tensor ACF. It can be directly obtained from Eq. (2) by using

$$G(t) = \sum_i m_i {r_i}^\alpha(t){v_i}^\beta(t)\,,$$
$$\dot{G}(t) = V P_{\alpha\beta}(t) = \sum_i m_i v_i^\alpha v_i^\beta + \frac{1}{2}\sum_{i\neq j} F_{ij}^\alpha r_{ij}^\beta\,, \quad (4)$$

which gives

$$\eta_{\alpha\beta} = \lim_{t\to\infty} \frac{1}{VK_BT}\frac{1}{2t}\left[\sum_i m_i({r_i}^\alpha(t){v_i}^\beta(t) - {r_i}^\alpha(0){v_i}^\beta(0))\right]^2, = \frac{V}{K_BT}\int_0^\infty \langle P_{\alpha\beta}(t_0)P_{\alpha\beta}(t_0+t)\rangle_{t_0}dt, \quad (5)$$

where $\eta_{\alpha\beta}$, V, T, K_B, m_i are viscosity tensor component, volume, temperature, Boltzmann constant, and atomic mass of particle i, respectively [20]. The summations are taken over all atoms, and F_{ij}^α and r_{ij}^α represent the specified component of the force and distance between ith and jth atoms, respectively. The expression $P_{\alpha\beta}$ is defined as the microscopic stress tensor in the form of the virial equation [25]. The viscosity of bulk water is subsequently evaluated from averaging over the time ACF of the off diagonal components of this symmetric tensor that include three possible $\alpha\beta$ permutations ($\alpha \neq \beta = x, y, z$) aiming to reduce the statistical error [26]. We use the GK method to calculate the viscosity [Eq. (5)]. There are also other alternatives using either equilibrium or nonequilibrium MD simulations which have some technical limitations. For instance, using the nonequilibrium approach, the obtained viscosity was found to be highly sensitive to the velocity profile of the flowing water molecules [6,27]. The stress tensor components in our simulations were calculated using the LAMMPS routines [15].

Transport properties in the presence of confinement, due to inhomogeneities of density, induced by the graphene capillary are not equal along the lateral (x and y) and the perpendicular (z) directions. When the confinement is removed, all corresponding components converge to their bulk values. In the presence of confinement, the diffusion coefficient, D_α along the perpendicular direction is insignificant, i.e., $D_z \ll D_x, D_y$. Here we report the lateral diffusion coefficient, i.e., the diffusion coefficient for the confined system is given by $D = (D_x + D_y)/2$.

In order to calculate the viscosity, we define two different components as follows

$$\eta_{xy}, \quad \eta_z = \tfrac{1}{2}(\eta_{xz} + \eta_{yz}), \quad (6)$$

where η_{xy} and η_z are the in-plane (along the channel) and lateral shear (perpendicular to the channel) viscosities, respectively [28]. We will show that both η_{xy} and η_z are affected by the confinement and $\eta_z < \eta_{xy}$. Since the viscosity is a collective property rather than a property of a single molecule, we would expect that the corresponding numerical results using Eq. (5) are less accurate as compared to the diffusion coefficient [8] due to the lack of extra atomic averaging $\langle\,\rangle_i$ present in Eq. (3). In MD simulations, an accurate calculation of the ACF tail is very demanding when evaluating the viscosity, hence we used the upper limit of 1 ps in Eq. (5) taking one sample per 2 fs [17].

Friction coefficient between solid/fluid interface is obtained by linear response theory and the Mori-Zwanzig formalism based on the force auto-correlation function [17,29].

$$\xi_\alpha = \frac{1}{SK_BT}\int_0^\infty \langle F^\alpha(t_0)F^\alpha(t_0+t)\rangle_{t_0}dt, \quad (7)$$

here S stands for interfacial area and F^α refers to the total force for each of the lateral components ($\alpha = x, y$) acting on the solid due to the fluid. In our simulations, the friction factor ξ was obtained by averaging over the lateral components and the two graphene surfaces.

Then, from the definition of viscosity, we can also define the relevant components for the slip length of water confined between graphene oxide layers as

$$L_{xy} = \frac{\eta_{xy}}{\xi}, \quad L_z = \frac{\eta_z}{\xi}. \quad (8)$$

Where, the z component has a significant contribution to the water flow through the nanocapillaries. The slip length is the distance into the surface at which the tangent to the fluid velocity becomes zero in a field driven flow. It characterizes the degree of interfacial friction which depends on the molecular structure of the surface and the fluid. For a given driving force, it defines the slip velocity over the surface and a rough estimate of the Navier slip length is given by η/ξ.

III. SURFACE CHARGE EFFECTS

Nanoconfinement changes the intrinsic properties of water and the interfacial coefficients. Here, we report results for the variation of the diffusion coefficient, viscosity, friction coefficient, and slip length with the height of the channel (h) for pure water confined between charged graphene surfaces.

A. Diffusion coefficient

In general, confinement suppresses the diffusion coefficient [30]. We found that the diffusion coefficient oscillates as a function of the thickness of the water layer due to commensurability effects [6]. In Fig. 2, we show the variation of D versus h in semilog scale for graphene sheets with three different surface charge densities, $\sigma = 0$, 0.1, and 1 e nm^{-2}. These densities correspond to typical charge densities observed over carbon and hexagonal boron nitride nanotubes [31,32]. When there is no surface charge, the calculated diffusion coefficient oscillates for small h. A sudden drop in D (about

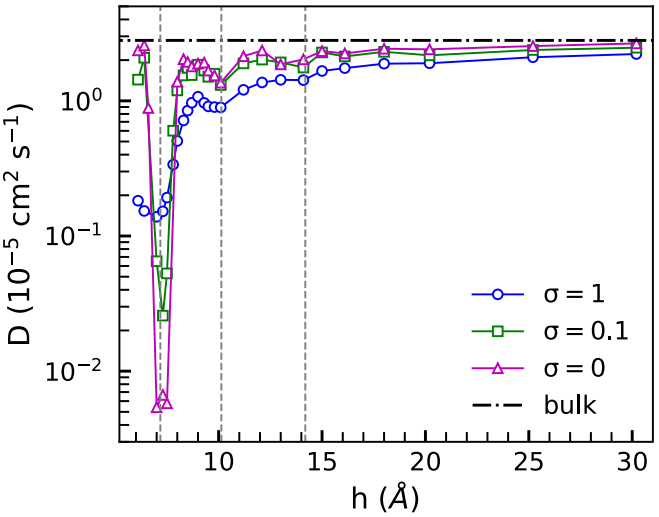

FIG. 2. The variation of the diffusion coefficient with respect to the graphene capillaries gap in semilog scale for different surface charge densities of $\sigma = 0$, 0.1, and 1 e nm^{-2}. The commensurability of confined water (dashed vertical lines) leads to oscillatory variations in diffusion coefficient for $h < 20$ Å.

two orders of magnitude) was found for $h = 7.0$ Å which is attributed to a 2D solidification of water at commensuration of the water molecule sizes and the channel gap distance [6,33]. The exact value of the slid size depends slightly on the particular used force field. In contrast to Ref. [8], here we found that the diffusion coefficient oscillates and is very sensitive to the height of the channel which is consistent with our previous work [6]. The horizontal dash-dotted line in Fig. 2 corresponds to our calculated diffusion coefficient for bulk water, i.e., 2.83 cm^2 s^{-1}, which is in good agreement with previous reports 2.79–3.02 cm^2 s^{-1} [34]. In the presence of surface charges, e.g., $\sigma = 1$ e nm^{-2}, the water molecules near the surface of the confining walls are bonded to the charged sites causing D to decrease, and it reduces the amplitude of the oscillations. Comparison between the diffusion coefficient of neutral and charged surfaces reveals that the surface charge increases the water diffusion for $h \sim 8$ Å while it decreases beyond this threshold. As one naturally expects, by increasing h, the diffusion coefficient very quickly approaches the bulk value.

B. Viscosity

In Fig. 3, we depict the variation of η_{xy} and η_z [Eq. (6)] with the height of the channel. The dash-dotted line represents our computed η for bulk water 6.6×10^{-4} Pa s which agrees with the reported value of 6.72×10^{-4} Pa s obtained using the same SPC/E model [23]. In the absence of surface charges, we found that in-plane viscosity η_{xy} shows similar oscillations at small separation distances which is consistent with our previous work [6], see Fig. 3(a). Interestingly, we found a maximum of η_{xy} at 7.0 Å which corresponds to the minimum in D (Fig. 2). The lateral component of viscosity η_z is insignificant for small gap distances and it drastically increases when confinement is gradually removed, see Fig. 3(b), except for $\sigma = 1$ e nm^{-2}. The latter is due to the stronger adhesion between water and the charged surface and it is larger than the bulk value. For instance, at $h = 15$ Å we found $\eta_{xy}^{[\sigma=1]} \approx \eta_z^{[\sigma=1]}$, and the ratios $\eta_z^{[\sigma=1]}/\eta_z^{[\sigma=0]} = 55$ and $\eta_z^{[\sigma=0.1]}/\eta_z^{[\sigma=0]} = 11$ which shows that surface charges strongly enhance η_z. Moreover, the two viscosity components decrease in the presence of surface charges which indicates that the interaction with the surface has a larger effect than confinement. Our results indicate that adding surface charges increases the viscosity components at small separation distance while they approach the bulk value for large h.

C. Friction coefficient

We further calculated the friction coefficient for confined water using Eq. (7). The results are shown in Fig. 4 for three typical charge surface densities. Our calculated ξ for pure water (2.3×10^4 N s m^{-3}) over neutral surfaces is close to the recently reported value of 2.0×10^4 N s m^{-3} for $h = 50$ Å [17]. The surface charge enhances the water/graphene interfacial attraction, and as a result, the friction coefficient ξ increases with up to two orders of magnitude. A noticeable oscillatory behavior can also be seen for $\sigma = 0$ and even $\sigma = 0.1$ e nm^{-2}. For small h, the friction σ increases very strongly which is due

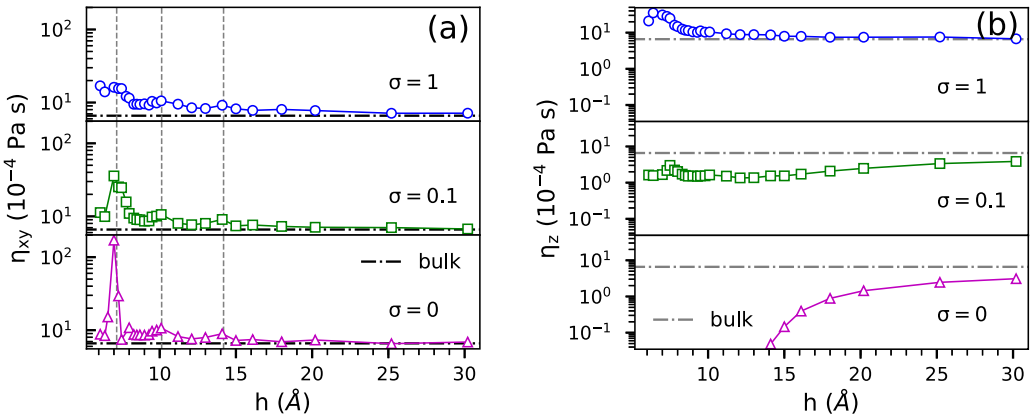

FIG. 3. The variation of the components of viscosity (a) η_{xy}, and (b) η_z as a function of the graphene capillary gap distance in semilog scale for different surface charge densities, i.e., $\sigma = 0$, 0.1, and 1 e nm^{-2}. The dash-dotted line refers to the viscosity of bulk water (6.72×10^{-4} Pa s). The vertical dashed lines indicate the commensurate distances.

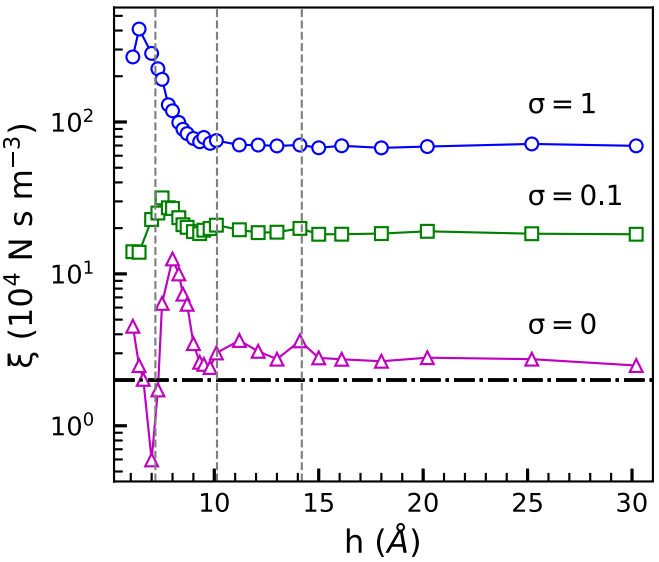

FIG. 4. The variation of the frictional coefficient ξ as a function of the graphene capillary gap distance in semilog scale for different surface charge densities of $\sigma = 0, 0.1$, and 1 e nm^{-2}. The dash-dotted line represents the reported ξ (2.0×10^4 N s m^{-3}) for $h = 50$ Å [17].

to the stronger adhesion between water and the charged surfaces. For a given $h = 15$ Å, we can compare the frictional coefficient for different surface charges, i.e., $\xi^{[\sigma=1]}/\xi^{[\sigma=0]} = 24$ and $\xi^{[\sigma=0.1]}/\xi^{[\sigma=0]} = 6.5$ indicating the hydrophilicity of GO surfaces. It is also interesting to note that the larger the surface charge density, the less pronounced are the commensurability effects. The larger difference $\xi^{[\sigma=0.1]} - \xi^{[\sigma=0]}$ as compared to $\xi^{[\sigma=1]} - \xi^{[\sigma=0.1]}$ shows the strong impact of functional groups (over GO) on the interfacial friction coefficient.

IV. EFFECTS OF IONS

To investigate the effect of solvation we consider as an example Na^+ and Cl^- ions and study its effect on the dynamical properties of confined water. In agreement with previous works [35], we found that adding ions linearly decreases the diffusion coefficient while it increases the viscosity regardless of confinement. This can be attributed to the hydration effect of ions which decreases the mobility and suppresses the dynamics of the water molecules. Hydration is a crucial phenomenon in the water filtration process which is altered by nanosize confinement [7]. In Figs. 5(a) and 5(b), we plot the average number of water molecules $n(r)$ [Eq. (1)] near Na^+/Cl^- ions at radial distance r for few confinement distances: bulk, $h = 8$, 10, 20 Å. The number of H_2O at the first (n_1) and second (n_2) hydration shells are listed in Table I. It is seen that n_1 is not affected by h except for Cl^- at the very small slid size of 8 Å which is due to its relatively large effective atomic radius. Notice that confinement reduces drastically the number of water molecules in the second hydration shell (with about a factor of 2) which is an important parameter for water/ion permeation through GO capillaries [5].

We found that the presence of ions reduces the frictional coefficient. Figure 6 shows the variation of ξ with separation distance h for three different ion concentrations, i.e., 0, 1, and 5%. The dash-dotted line represents the reported ξ (2.0×10^4 N s m^{-3}) for $h = 50$ Å [17]. At large h the suppression of the friction due to the presence of ions is clear. For example, for 15 Å the decrease of ξ with ion concentration is $\xi^{[5\%]}/\xi^{[\text{pure}]} = 0.69$ and $\xi^{[1\%]}/\xi^{[\text{pure}]} = 0.91$. The reason is that when ions are present, they are surrounded by water molecules because of the hydration effect. As a result, the water molecules will contribute less to water-surface interactions. Moreover, we obtained similar fluctuations in the friction coefficient at small h due to the previously discussed commensurability effects.

V. CONCLUSIONS AND DISCUSSION

Our MD simulations revealed that the intrinsic dynamical properties of water strongly depends on the commensurability of water molecules encapsulated in graphene oxide capillaries. More importantly, the transport parameters exhibit oscillatory variations particularly when the confinement is less than 20 Å. At such commensurate states, confined water forms distinct layers which occurs at specific gap distances [6]. We found that almost all dynamical properties are affected by this commensurability effect. Table II quantifies the diffusion,

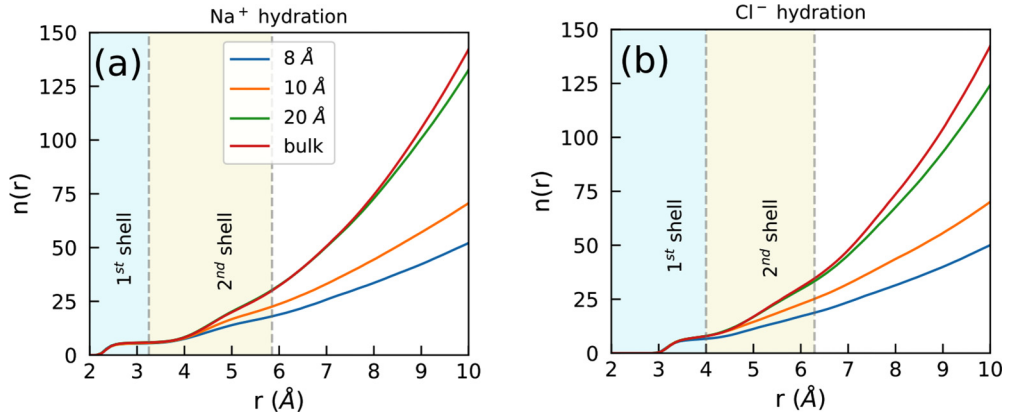

FIG. 5. The variation of the average number of water molecules $n(r)$ from Na^+ (a) and Cl^- (b) ions calculated by using Eq. (1) as a function of radial distance r for difference graphene interlayer distances. The two vertical dashed lines indicate the first and second hydration shells which are obtained from appropriate RDFs between ions and oxygen atoms of the water molecules.

TABLE I. The number of water molecules in the first and second hydration shell which are accumulated around Na^+ and Cl^- ions, see Figs. 5(a) and 5(b), for different confinement.

Ion	8 Å		10 Å		20 Å		bulk	
	n_1	n_2	n_1	n_2	n_1	n_2	n_1	n_2
Cl^-	6.5	12.3	8.2	16.9	8.2	24.3	8.2	26.7
Na^+	5.7	12.3	5.7	16.9	5.7	24.2	5.7	24.5

viscosities, frictional coefficient, and slip lengths for several selected confinement distances. It is important to note that all extrema occurs at the same interlayer distances that support the fact that commensurability underlies the oscillatory behaviors. The underlined red (double underlined blue) colored numbers represent the local maximum (minimum) in their corresponding figures. Here we considered only pure water without surface charges. By increasing the slid size commensurability disappears gradually and the results coincide with the bulk values.

The density profile along the confinement direction (z axis) is shown in Fig. 7 to demonstrate the commensurability. The graphs are shifted for different interlayer distances and the colored zones refer to the specific number of water layer. The red colors (6.1, 8.3, and 12.1 Å) represent the commensurate states with a distinct number of water layers, and the blue colors (7.0, 10.1, and 14.1 Å) refer to the state just before a new layer of water forms. Interestingly, the colored density profiles correspond to the extrema in the values of dynamical properties, see Table II. Moreover, the number of intra(inter)hydrogen bonds of the layers is an additional quantity that gives us similar information on the commensurability effect.

We calculate the slip lengths for all the above discussed cases using Eq. (8). The slip length is the distance at which

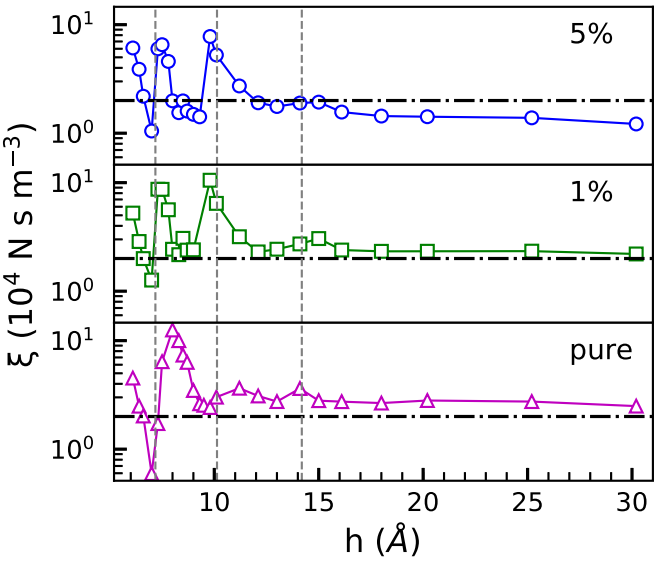

FIG. 6. The friction coefficient ξ as a function of nanocapillary distance for pure water, 1%, and 5% ion concentrations. The dash-dotted line represents the reported ξ (2.0×10^4 N s m^{-3}) for $h = 50$ Å [17].

TABLE II. Dynamical properties, i.e., diffusion, viscosities, frictional coefficient, and slip lengths for several selected confinement distances exhibiting oscillatory behaviors induced by the commensurability effect. The underlined gray (double underlined black) colored numbers represent the local maximum (minimum) values. For simplicity, we only consider pure water without surface charges.

h (Å)	6.1	7.0	8.3	10.1	12.1	14.1	20.2
D (10^{-5} cm^2 s^{-1})	2.3	0.005	2.0	0.03	2.3	0.14	2.4
η_{xy} (10^{-4} Pa s)	8.6	155	8.3	10	7.4	8.8	7.4
η_z (10^{-4} Pa s)						0.04	1.3
ξ (10^4 N s m^{-3})	4.5	0.5	1.4	3.0	3.1	3.6	2.7
L_{xy} (Å)	195	24457	59	377	150	250	263
L_z (Å)				0.27	2.95	1.40	48

the linearly extrapolated velocity reaches a no-slip condition. Figure 8(a) shows the two components of the slip length, L_{xy} and L_z, for different surface charge densities σ as a function of the slid size. When $\sigma = 0$ and for large h, our obtained slip lengths for L_{xy} (250 Å) and L_z (200 Å) are comparable with the reported values of 290 Å [17] (dash-dotted line) for bulk water over graphene. Note that in recent studies [14,17], a constant

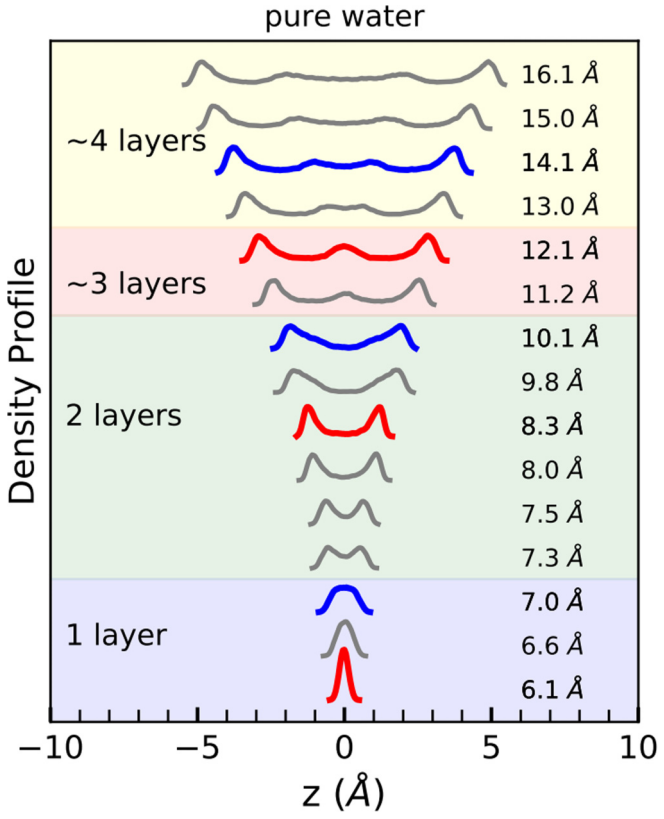

FIG. 7. Density profile of oxygen atoms along the confinement direction (z axis) for pure water without surface charges. The graphs are shifted for the different interlayer distances and the colored zones refer to the numbers of water layer. The red color (6.1, 8.3, and 12.1 Å) represent the commensurate states with distinct water layers, and the blue colors (7.0, 10.1, and 14.1 Å) refer to the state just before a new water layer forms.

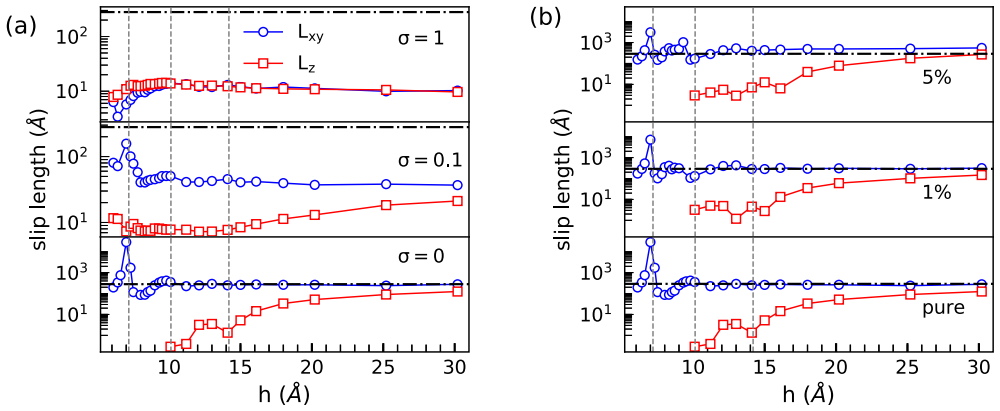

FIG. 8. Components of the slip length L_{xy} and L_z for different surface charge densities of $\sigma = 0$, 0.1, and 1 e nm^{-2} (a) and for pure water, 1%, and 5% ion concentrations (b). The dash-dotted line indicates the reported hydrodynamic slip length (280 Å) for a gap distance of 30 Å [17].

bulk viscosity was assumed in the calculation of the slip length even for small gap distance, i.e., $h < 30$ Å. If we use the bulk viscosity (6.72×10^{-4} Pa s) in the numerator of the slip length equation namely η/ξ without taking into account the impact of confinement, we found $L = 285$ Å which is in agreement with their reported slip length. In order to find a h-dependent slip length, we include the effects of confinement to both viscosity and friction coefficient. We found that L_{xy} fluctuates particularly at small h, however, L_z is much smaller at small distances, i.e., $h < 15$ Å, while it rapidly increases to the bulk value, see Fig. 8. In the presence of surface charges, slip lengths drastically reduce due to the fact that water molecules bind to the graphene surfaces. This is qualitatively in agreement with the experimental results for GO with oxygen groups [36]. It was also reported that a GO with 20% oxygen groups has a slip length of two orders of magnitude smaller than that over a graphene sheet which is comparable with our results shown in Fig. 7(a) [36,37]. In fact water permeability through a GO membrane is very complicated, for instance the water permeating through nanochannels made of GO is controlled by the size, structure, and distribution of pores as well as the length of the channels [36]. We argue that when water is confined in a nanocapillary with Angstrom scale size, the major influence on the slip length is due to L_{xy} while L_z is much more sensitive to channel height.

The slip length components for different ion concentrations of Na^+/Cl^- 0, 1, 5% are shown in Fig. 8(b) which reveal only a small influence of the presence of ions. The effect is considerable for large concentration if we compare the two top panels of Fig. 8(b) with the bottom one. Recently, Abraham *et al.* [5] studied the importance of the size of ions and its corresponding hydration. They found that water molecules stabilize ions by forming concentric hydration shells such that when an ion enters a channel some water molecules must be removed from the hydration shell leading to the effect that if ions are weakly bound by water molecules, they can easier enter into nanochannels. Here, we did not study the entrance barrier of the channels, instead we focused on the dynamical properties and resistance against diffusion of the ions inside the channel. Therefore, our results represented in Fig. 8(b) are not directly comparable with experimental results [5]. However, it is seen that by increasing the concentration of ions the slip length slightly decreases and the sensitivity of the hydration shell to the channel size is shown in Figs. 5(a) and 5(b), which are consistent with recent experiments [5,38]. It would also be interesting to note that GO membrane spacings can be controlled by certain type of cations (e.g., K^+) which can efficiently and selectively exclude permeation of other cations that have larger hydrated volumes [38].

Finally, we conclude that the concentration of ions does not dramatically change the slip length (this is relevant for recent experiments where the effects of ions with different hydrated diameters were found to be minimal [7]) while surface charges on the graphene surface and commensurability induced by confinement have a profound influence on the dynamical properties. The significant variation of the slip length with respect to the microscopic details of nanocapillaries and the complexity of the problem shows that more studies are needed (see Appendix). Our predictions of large slip lengths for water flow through charged nanocapillaries and in the presence of ions provide an important contribution to the field of nanofluidics and gives more insights on the underlying physics.

ACKNOWLEDGMENTS

We acknowledge fruitful discussions with Andre K. Geim, Irina Grigorieva, and Rahul R. Nair. This work was supported by the Flemish Science Foundation (FWO-Vl) and the Methusalem program.

APPENDIX

We performed several extra MD simulations in order to validate how close our simple model, based on surface charges, is to describe more real graphene oxide nanocapillaries. For comparative reason, we simulated two systems, one with excessive surface charges and the other containing functional groups, i.e., epoxy (O-) and hydroxyl (OH-) using a similar setup as discussed in the model and method sections of the

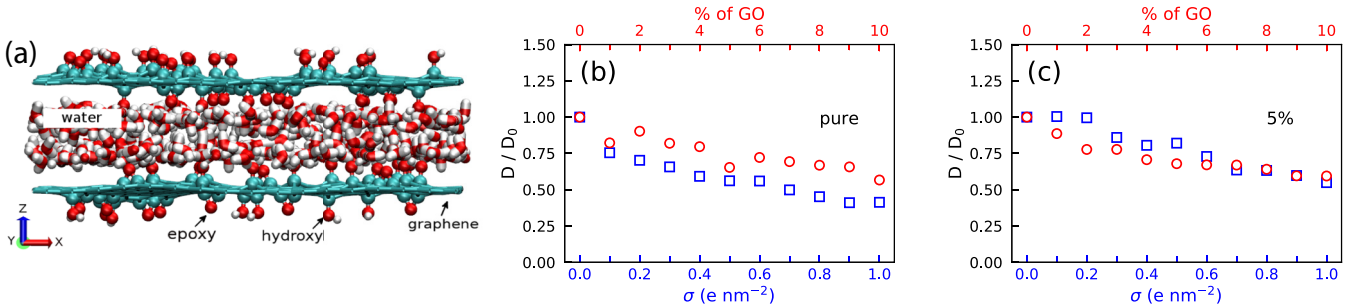

FIG. 9. Side view snapshot of water and graphene oxide nanocapillary containing epoxy and hydroxyl functional groups implemented by OPLS potentials (a). For comparative reason, the diffusion coefficient, as a typical dynamical property, is obtained for pure water (b) and water with 5% ion concentration (c) using our surface charges model and OPLS. Both results are very close supporting the use of our charge surface model (blue bottom scale) to describe the impact of functional groups (red top scale) over GO surface. The scale D_0 refers to the diffusion factor of pristine graphene, and the average capillary interlayer distance is 1 nm.

main text. The O- and OH- groups are randomly added to both sides of the graphene sheets, and they are not allowed to diffuse during simulations. We assumed that the functional groups have at least a radial distance of 3 Å. We introduce the ratio n_O/n_C, where n_O and n_C stand for the number of oxide sites and carbon atoms, respectively [see Fig. 9(a)], in order to make a link with the synthesis of graphene oxide reported in experiments [39]. The same SPC/E model [16] employed for water molecules and optimized potentials for liquid simulations (OPLS) has been used for the functional groups that contains bonds, angles, dihedrals, and nonbonded interactions [40]. The water-GO interaction was described by LJ 6-12 and Coulomb pair potentials [40]. Furthermore, the adaptive intermolecular reactive empirical bond order (AIREBO) potential was used for the graphene layers [41]. The graphene oxide layers are free to move with average separation distance of 1 nm, and the total density of 1 g cm^{-3} of water was obtained after relaxing the system.

In Figs. 9(b) and 9(c), we depict the variation of the diffusion coefficient of pure water and 5% concentrations as a function of n_O/n_C for graphene oxide (red top scale) and compared it with those obtained from varying surface charge density σ (blue bottom scale). The results are very close which justifies the use of our more simple model in this work. As a result, replacing functional groups with charges over the graphene surface is a physically meaningful simplification in modeling and simulating the dynamical properties of water inside GO membranes.

Figures 10(a) and 10(b) show a comparison of the corresponding density profiles of pure water and water with 5% ion concentration along the confinement direction for the excessive surface charge model (solid blue lines) and the OPLS model (dashed red lines). The results indicate that both are almost the same and commensurability exists in the latter model albeit it is a little suppressed due to the presence of functional groups between the surface and water.

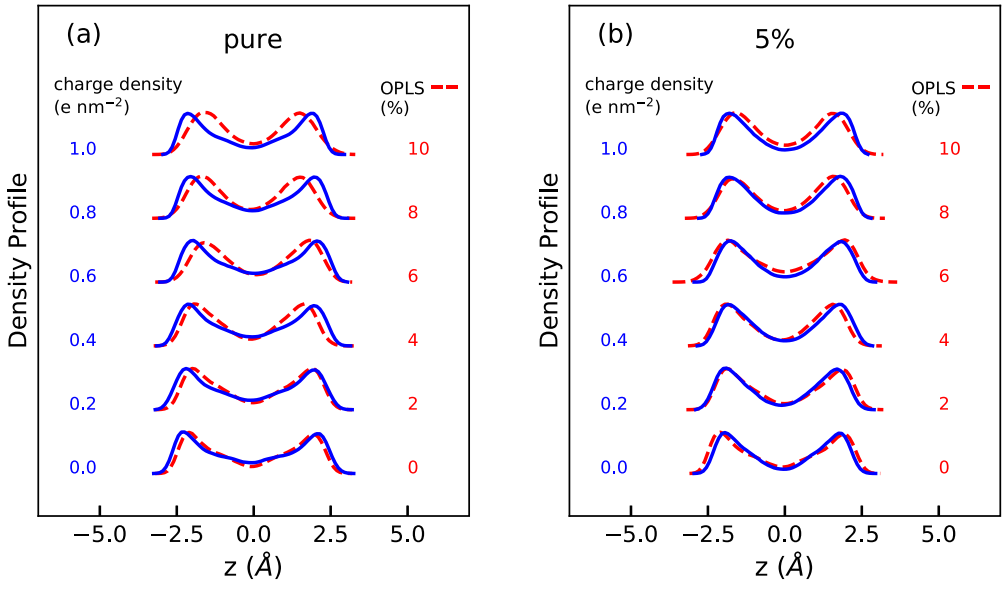

FIG. 10. Corresponding density profiles of oxygen atoms in water along the confinement direction (z axis) of pure water (a) and 5% ion concentration (b) are evaluated from the surface charge density model (solid blue lines) and the model with functional groups coverage (dashed red lines). The graphs for each surface charge density (functionals) are shifted.

[1] G. Hummer, J. C. Rasaiah, and J. P. Noworyta, Nature (London) **414**, 188 (2001).

[2] M. Majumder, A. Siria, and L. Bocquet, MRS Bull. **42**, 278 (2017).

[3] R. R. Nair, H. A. Wu, P. N. Jayaram, I. V. Grigorieva, and A. K. Geim, Science **335**, 442 (2012).

[4] H. W. Kim, H. W. Yoon, S. M. Yoon, B. M. Yoo, B. K. Ahn, Y. H. Cho, H. J. Shin, H. Yang, U. Paik, S. Kwon *et al.*, Science **342**, 91 (2013).

[5] J. Abraham, K. S. Vasu, C. D. Williams, K. Gopinadhan, Y. Su, C. Cherian, J. Dix, E. Prestat, S. J. Haigh, I. V. Grigorieva *et al.*, Nat. Nanotechnol. **12**, 546 (2017).

[6] M. Neek-Amal, F. M. Peeters, I. V. Grigorieva, and A. K. Geim, ACS Nano **10**, 3685 (2016).

[7] A. Esfandiar, B. Radha, F. C. Wang, Q. Yang, S. Hu, S. Garaj, R. R. Nair, A. K. Geim, and K. Gopinadhan, Science **358**, 511 (2017).

[8] Y. Liu and Q. Wang, Phys. Rev. B **72**, 085420 (2005).

[9] B. Radha, A. Esfandiar, F. C. Wang, A. P. Rooney, K. Gopinadhan, A. Keerthi, A. Mishchenko, A. Janardanan, P. Blake, L. Fumagalli *et al.*, Nature (London) **538**, 222 (2016).

[10] H. Li, Z. Song, X. Zhang, Y. Huang, S. Li, Y. Mao, H. J. Ploehn, Y. Bao, and M. Yu, Science **342**, 95 (2013).

[11] R. K. Joshi, P. Carbone, F. C. Wang, V. G. Kravets, Y. Su, I. V. Grigorieva, H. A. Wu, A. K. Geim, and R. R. Nair, Science **343**, 752 (2014).

[12] S. Sahu and M. Zwolak, Phys. Rev. E **98**, 012404 (2018).

[13] S. K. Kannam, B. D. Todd, J. S. Hansen, and P. J. Daivis, J. Chem. Phys. **138**, 094701 (2013).

[14] N. Wei, X. Peng, and Z. Xu, Phys. Rev. E **89**, 012113 (2014).

[15] S. Plimpton, J. Comput. Phys. **117**, 1 (1995).

[16] H. J. C. Berendsen, J. R. Grigera, and T. P. Straatsma, J. Phys. Chem. **91**, 6269 (1987).

[17] B. Ramos-Alvarado, S. Kumar, and G. P. Peterson, Phys. Rev. E **93**, 023101 (2016).

[18] S. Chowdhuri and A. Chandra, J. Chem. Phys. **115**, 3732 (2001).

[19] J. P. Ryckaert, G. Ciccotti, and H. J. Berendsen, J. Comput. Phys. **23**, 327 (1977).

[20] B. J. Alder, D. M. Gass, and T. E. Wainwright, J. Chem. Phys. **53**, 3813 (1970).

[21] A. P. Lyubartsev and A. Laaksonen, J. Phys. Chem. **100**, 16410 (1996).

[22] M. A. González and J. L. F. Abascal, J. Chem. Phys. **132**, 096101 (2010).

[23] G. S. Fanourgakis, J. S. Medina, and R. Prosmiti, J. Phys. Chem. A **116**, 2564 (2012).

[24] V. A. Levashov, J. Chem. Phys. **147**, 184502 (2017).

[25] E. N. Parker, Phys. Rev. **96**, 1686 (1954).

[26] S. Viscardy and P. Gaspard, Phys. Rev. E **68**, 041204 (2003).

[27] B. Hess, J. Chem. Phys. **116**, 209 (2002).

[28] M. H. Köhler and L. Barros da Silva, Chem. Phys. Lett. **645**, 38 (2016).

[29] L. Bocquet and J. L. Barrat, Phys. Rev. E **49**, 3079 (1994).

[30] H. Qiu and W. Guo, Phys. Rev. Lett. **110**, 195701 (2013).

[31] E. Secchi, A. Nigués, L. Jubin, A. Siria, and L. Bocquet, Phys. Rev. Lett. **116**, 154501 (2016).

[32] A. Siria, Ph. Poncharal, A. L. Biance, R. Fulcrand, X. Blase, S. T. Purcell, and L. Bocquet, Nature (London) **494**, 455 (2013).

[33] M. Sobrino Fernandez Mario, M. Neek-Amal, and F. M. Peeters, Phys. Rev. B **92**, 245428 (2015).

[34] P. Mark and L. Nilsson, J. Phys. Chem. A **105**, 9954 (2001).

[35] D. W. McCall and D. C. Douglass, J. Phys. Chem. **69**, 2001 (1965).

[36] H. Huang, Z. Song, N. Wei, L. Shi, Y. Mao, Y. Ying, L. Sun, Z. Xu, and X. Peng, Nat. Commun. **4**, 2979 (2013).

[37] N. Wei, X. Peng, and Z. Xu, ACS Appl. Mater. Interfaces **6**, 5877 (2014).

[38] L. Chen, G. Shi, J. Shen, B. Peng, B. Zhang, Y. Wang, F. Bian, J. Wang, D. Li, Z. Qian *et al.*, Nature (London) **550**, 380 (2017).

[39] D. R. Dreyer, S. Park, C. W. Bielawski, and R. S. Ruoff, Chem. Soc. Rev. **39**, 228 (2010).

[40] H. Tang, D. Liu, Y. Zhao, X. Yang, J. Lu, and F. Cui, J. Phys. Chem. C **119**, 26712 (2015).

[41] S. J. Stuart, A. B. Tutein, and J. A. Harrison, J. Chem. Phys. **112**, 6472 (2000).